JOURNAL OF GEOPHYSICAL RESEARCH, VOL. 106, NO. A11, PAGES 25,873–25,889, NOVEMBER 1, 2001

Magnetic impulse event: A detailed case study of extended ground and space observations

R. Kataoka,[1,2] H. Fukunishi,[1] L. J. Lanzerotti,[2] C. G. Maclennan,[2] H. U. Frey,[3] S. B. Mende,[3] J. H. Doolittle,[4] T. J. Rosenberg,[5] and A. T. Weatherwax [5]

Abstract. Analysis of conjugate data from extended magnetometer networks in northern and southern high latitudes is used to elucidate the initiation and the evolution of a magnetic impulse event (MIE) on June 6, 1997. In addition, data from all-sky imagers, imaging riometers, and Super Dual Auroral Radar Network radars in Antarctica are investigated to confirm the energy content, motion, and electrical current structure of the MIE. The MIE was accompanied by traveling convection vortices (TCVs) that began at ~10 MLT and moved eastward (toward dusk) and slightly equatorward at 1-3 km/s across the noon meridian with north-south conjugacy. The MIE had upward field-aligned currents with soft electron precipitation that was located near the trailing edge of the Hall current loop. During the MIE interval the interplanetary magnetic field (IMF) was directed strongly outward from the Sun (B_x = -5 nT), with a slightly positive (1-2 nT) B_z, and a nearly zero B_y. Since abrupt solar wind pressure changes are unlikely under this IMF orientation (and none was, in fact, observed), classical mechanisms for MIE generation, such as a pressure pulse or dayside reconnection, are excluded. It is speculated that an abrupt IMF cone angle change from 60° to 20°, ~30 min prior to the MIE onset, may have been an indirect trigger of this event via the interaction between the solar wind and the bow shock.

1. Introduction

The mechanisms by which energy and momentum are transferred from the solar wind into the Earth's magnetosphere to produce phenomena ranging from the aurora to high-energy trapped particle radiation continue to be important subjects of investigations in space plasma physics. Two areas of research that have had much attention paid to them concern energy transfer at the dayside magnetopause by magnetic reconnection and by changes in the dynamic pressure of the solar wind as it impinges upon the magnetosphere (see, e.g., very early work by *Dungey* [1961] and *Tamao* [1964]). Most relevant to this paper are the studies in the last decade or so of transient disturbances in the geomagnetic field at very high geomagnetic latitudes. These transients are called magnetic impulse events (MIEs). It has been shown that some MIEs can be interpreted in terms of traveling convection vortices (TCVs) moving antisunward from the midday sector [e.g., *Friis-Christensen et al.*, 1988; *Glassmeier et al.*, 1989].

Most investigators have concluded that MIEs are produced by field-aligned electrical currents in the Earth's high latitudes. A number of investigators have asserted that perhaps the majority of these events are caused by magnetic reconnection at the Earth's magnetopause [e.g., *Goertz et al.*, 1985; *Lanzerotti et al.*, 1986, 1987, 1990; *Lanzerotti*, 1988; *Sandholt et al.*, 1990; *Bering et al.*, 1990; *Pinnock et al.*, 1991; *McHenry and Clauer*, 1987; *Lockwood et al.*, 1988; *Konik et al.*, 1994, 1995; *Lin et al.*, 1995]. *Konik et al.* [1994], on the basis of a careful statistical study, concluded that magnetic reconnection is likely to be responsible for generating a minimum of 50%-70% to a maximum of 90% of the MIEs selected by their criteria. At the same time, other investigators have challenged this interpretation, claiming that dynamic pressure changes in the solar wind or magnetosheath can account for the high-latitude MIE signatures [e.g., *Friis-Christensen et al.*, 1988; *Potemra et al.*, 1989; *Farrugia et al.*, 1989; *Sibeck*, 1990, 1992, 1993; *Sibeck and Croley*, 1991; *Sibeck and Korotova*, 1996; *Korotova et al.*, 1997; *Lühr et al.*, 1998; *Moretto et al.*, 1997; *Vorobjev et al.*, 1999].

Theoretical support for both options exists, as might be expected. The basic idea for field-aligned currents driven by dynamic pressure changes derives from the early work of *Tamao* [1964], who attempted to define the ground signatures of storm sudden commencements (SSCs). Follow-on works have been published by several investigators, including *Kivelson and Southwood* [1991] and *Glassmeier and Heppner* [1992]. The generation of field-aligned currents by magnetic reconnection has been theoretically discussed by several groups as well, including *Saunders et al.* [1984], *Lee and Fu* [1985], and *Southwood* [1985, 1987].

Uncertainty (and some controversy) on the origin(s) and evolutionary dynamics of MIEs still exists. The importance of the problem still exists as well. A major portion of the difficulty in obtaining closure is that there is no agreed-upon "standard" for defining the occurrence or existence of a MIE. The work of *Konik et al.* [1994] used very strict criteria of event amplitude and duration based principally upon the idea that the time variation in the vertical component magnetic field was the defining feature of the field-aligned currents, while at the same time keeping in mind the Fukushima theorem [*Fukushima*,

[1]Department of Geophysics, Tohoku University, Sendai, Japan.
[2]Bell Laboratories, Lucent Technologies, Murray Hill, New Jersey.
[3]Space Sciences Laboratory, University of California, Berkeley, California.
[4]Lockheed Martin Palo Alto Research Laboratory, Palo Alto, California.
[5]Institute for Physical Science and Technology, University of Maryland, College Park, Maryland.

Paper number 2000JA000314.
0148-0227/01/2000JA000314$09.00

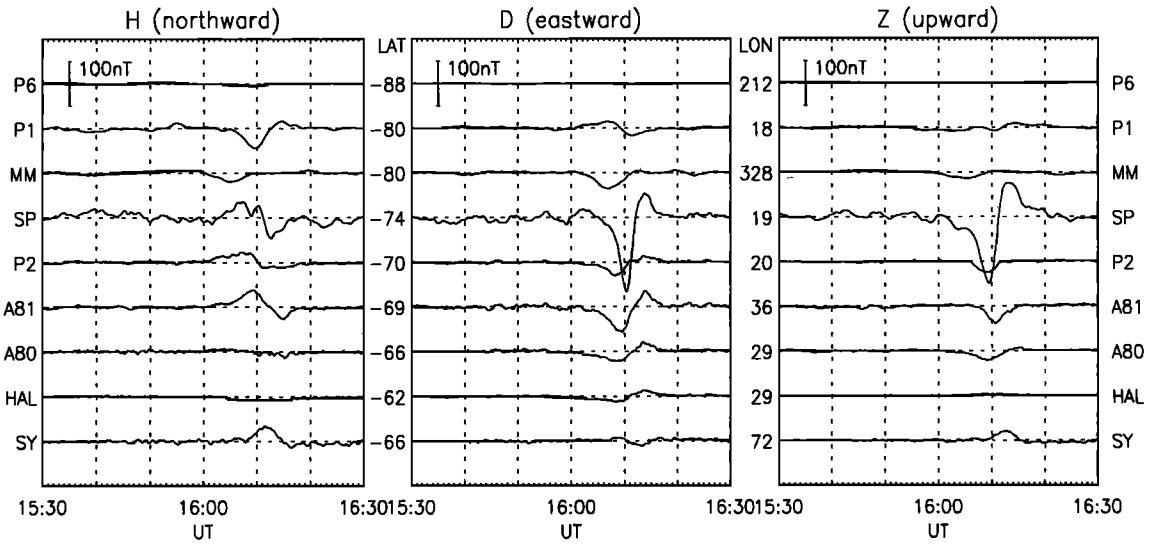

Figure 1. Three components of ground-based geomagnetic field data obtained at nine sites in the Antarctic (Southern Hemisphere) between 1530 UT and 1630 UT on June 6, 1997. A magnetic impulse event (MIE) is most evident at South Pole station with amplitudes of 150 and 160 nT in the *Z* and *D* components, respectively.

1969]. However, many other investigations have not used the vertical component variations in their work, because the vertical component can be affected by ground induction effects.

A minor difficulty has been that most investigations have, of necessity, used a limited spatial extent of geomagnetic observations. All investigators have well recognized such experimental limitations on their work. Indeed, one of the driving factors for implementing new observational programs such as the Magnetic Array for Cusp and Cleft Studies (MACCS) in northern Canada [*Hughes and Engebretson*, 1997] and the International Monitor for Auroral Geomagnetic Effects (IMAGE) array in northern Europe [e.g., *Lühr and Blawert*, 1994] has been to acquire spatial information on MIEs and TCVs. The U.S. automatic geophysical observatories (AGOs) in the Antarctic [*Rosenberg and Doolittle*, 1994], together with some populated stations, were intended to provide a similar, but less extensive, two-dimensional array in the Southern Hemisphere. *Sato et al.* [1999] used the U.S. AGOs (as well as South Pole and McMurdo stations) for the first time to delineate the scale sizes of several MIEs in the Southern Hemisphere.

The purpose of this paper is to demonstrate the initiation and evolution of the MIE on June 6, 1997, using conjugate analysis of magnetometer network data from northern and southern high latitudes. Data sets from all-sky imagers, imaging riometers, and Super Dual Auroral Radar Network (SuperDARN) radar in Antarctica are also investigated to confirm the energy content, motion, and electrical current structure of the MIE.

2. Magnetic Impulse Event

The magnetic impulse event analyzed herein is shown in Figure 1, which plots the 10-s-averaged local geomagnetic south-north, west-east, and vertical (*H*, *D*, and *Z*, respectively) component magnetic field traces for the interval 1530-1630 UT on June 6, 1997, for nine Antarctic stations. The geomagnetic signature at the near-cusp station SP (South Pole) is a classic MIE signature according to the criteria of *Konik et al.* [1994] [see also *Lanzerotti et al.*, 1991]. Out of a rather quiet background a sudden impulse appears at ~1610 UT in the *Z* component magnetic field with an amplitude ~150 nT. The amplitude in the *D* component is also large, ~160 nT, while the *H* component is much smaller. The *H* trace appears to be composed of two components: a pulse train and a soliton, the soliton being of similar (but inverted) character to the impulses in the *D* and *Z* components. This interval was geomagnetically quiet, with $Kp = 1+$ and $\Sigma Kp = 13$ for the previous 24 hours. The principal reason this event was selected for a detailed case study is that auroral image data from multiple optical sites covering the dayside cusp, the low-latitutde boundary layer (LLBL), and the polar cap region are available. Some research on MIEs has already made use of optical data, generally from single locations, to examine the particle precipitation accompanied by MIEs [*Fukunishi and Lanzerotti*, 1989; *Mende et al.*, 1990; *Sandholt et al.*, 1990; *Vorobjev et al.*, 1994; *Lühr et al.*, 1996]. These reports provide evidence that the events appear to coincide with structured field-aligned electrical currents that are directed out of the ionosphere. However, MIEs can propagate over long distances, at least more than ~1000 km that corresponds to the field of view of one all-sky imager. Images from the U.S. AGO all-sky imager network and populated stations make it possible to trace the propagation of MIE-related aurora over longer distances. Such data provide important additional information on the energy content, motion, and electrical current structure of MIEs. Since this event occurred almost at the southern winter solstice, optical data were available in the Southern Hemisphere.

3. Data Sets

An extensive set of ground- and space-based data were examined, consulted, and used in this investigation in order to provide as much information and insight as possible on the initiation and evolution of the MIE of June 6, 1997 (Figure 1). By examining in detail as much relevant geophysical data as can be assembled, we provide in this paper the first description of the generation and motion of a MIE in the Northern and Southern Hemispheres. The geophysical coordinates of the ground observatories are provided in Table 1.

Table 1. Geographic and geomagnetic coordinates of the observatories. [a]

Code	Stations	GLAT	GLON	MLAT	MLON	UT-MLT
		CANOPUS Magnetometer Chain				
SIM	Fort Simpson	61.8	238.8	67.6	291.9	0904
CON	Contwoyto Lake	65.8	248.8	73.4	301.9	0823
SMI	Fort Smith	60.0	248.1	67.8	304.6	0813
MCM	Fort Mcmurray	56.7	248.8	64.7	307.2	0804
RAB	Rabbit Lake	58.2	256.3	67.5	317.1	0727
TAL	Taloyoak	69.5	266.5	79.2	328.3	0646
RAN	Rankin Inlet	62.8	267.9	73.1	334.3	0627
ESK	Eskimo Point	61.1	266.0	71.4	331.4	0637
CHU	Fort Churchill	58.8	265.9	69.2	331.9	0635
ISL	Island Lake	53.9	265.3	64.4	331.9	0635
PIN	Pinawa	50.2	264.0	60.7	330.3	0640
		MACCS				
IG	Igloolik	69.3	278.2	79.2	352.5	0525
RB	Repulse Bay	66.5	273.8	76.7	344.1	0554
CH	Coral Harbour	64.1	276.8	74.5	349.9	0534
CD	Cape Dorset	64.2	283.4	74.3	1.6	0454
IQ	Iqualuit [b]	63.8	291.5	73.1	15.0	0406
		Greenland Magnetometers				
THL	Thule	77.5	290.8	85.5	33.9	0253
KUV	Kullorsuaq	74.6	302.8	81.3	44.8	0204
UPN	Upernavik	72.8	303.9	79.6	42.2	0215
UMQ	Umanaq	70.7	307.9	77.0	44.1	0206
GDH	Godhavn	69.3	306.5	75.9	40.5	0222
ATU	Attu	67.9	306.4	74.7	39.1	0228
STF	Sondre Stromfjord	67.0	309.3	73.3	41.8	0216
SKT	Sukkertoppen	65.4	307.1	72.1	38.0	0234
GHB	Godthab	64.2	308.3	70.7	38.6	0231
FHB	Frederikshab	62.0	310.3	68.1	39.7	0226
NAQ	Narsarsuaq	61.2	314.6	66.4	43.9	0206
NRD	Nord	81.6	343.3	80.9	106.3	2114
DMH	Danmarkshavn	76.8	341.4	77.3	87.4	2236
DNB	Daneborg	74.3	339.8	75.2	80.7	2307
SCO	Scoresbysund	70.5	338.0	71.7	73.4	2342
AMK	Ammassalik	65.6	322.4	69.4	54.7	0115
TJ	Tjornes [c]	66.2	342.9	66.5	73.0	2341
		Southern Hemisphere Magnetometers				
P6	U.S. AGO P6	-72.1	127.9	-87.8	212.2	1441
P1	U.S. AGO P1	-83.9	129.6	-80.1	17.6	0343
MM	Mcmurdo	-77.9	166.7	-80.0	327.7	0655
SP	South Pole	-90.0	0.0	-74.0	18.9	0335
P2	U.S. AGO P2	-85.7	313.6	-69.8	19.7	0328
A81	U.K. AGO A80	-81.5	3.0	-68.5	36.3	0218
A80	U.K. AGO A81	-80.8	339.6	-66.2	29.3	0246
HB	Halley	-75.6	333.6	-61.5	29.3	0243
SY	Syowa	-69.0	39.6	-66.1	71.9	2356

[a] Abbreviations are defined as follows: GLAT and GLON, geographic latitude and longitude, respectively; and MLAT and MLON, magnetic latitude and longitude, respectively (all in degrees); UT, universal time; MLT, magnetic local time; CANOPUS, Canadian Auroral Network for OPEN Program Unified Study; MACCS, Magnetic Array for Cusp and Cleft Studies; AGO, automatic geophysical observatories.

[b] Station is run by Bell Laboratories.

[c] Station is run by National Institute of Polar Research, Japan.

Plate 1. All-sky images (geomagnetic coordinates) of the 630.0-nm emissions seen overhead at stations MM and SP at 2-min intervals from (top left) 1556 UT to (bottom right) 1624 UT. The fields of view of all stations are shown, as is an outline of a portion of the Antarctic continent. Local noon is at the top of all panels; west is left and east is right in this view looking down onto Earth.

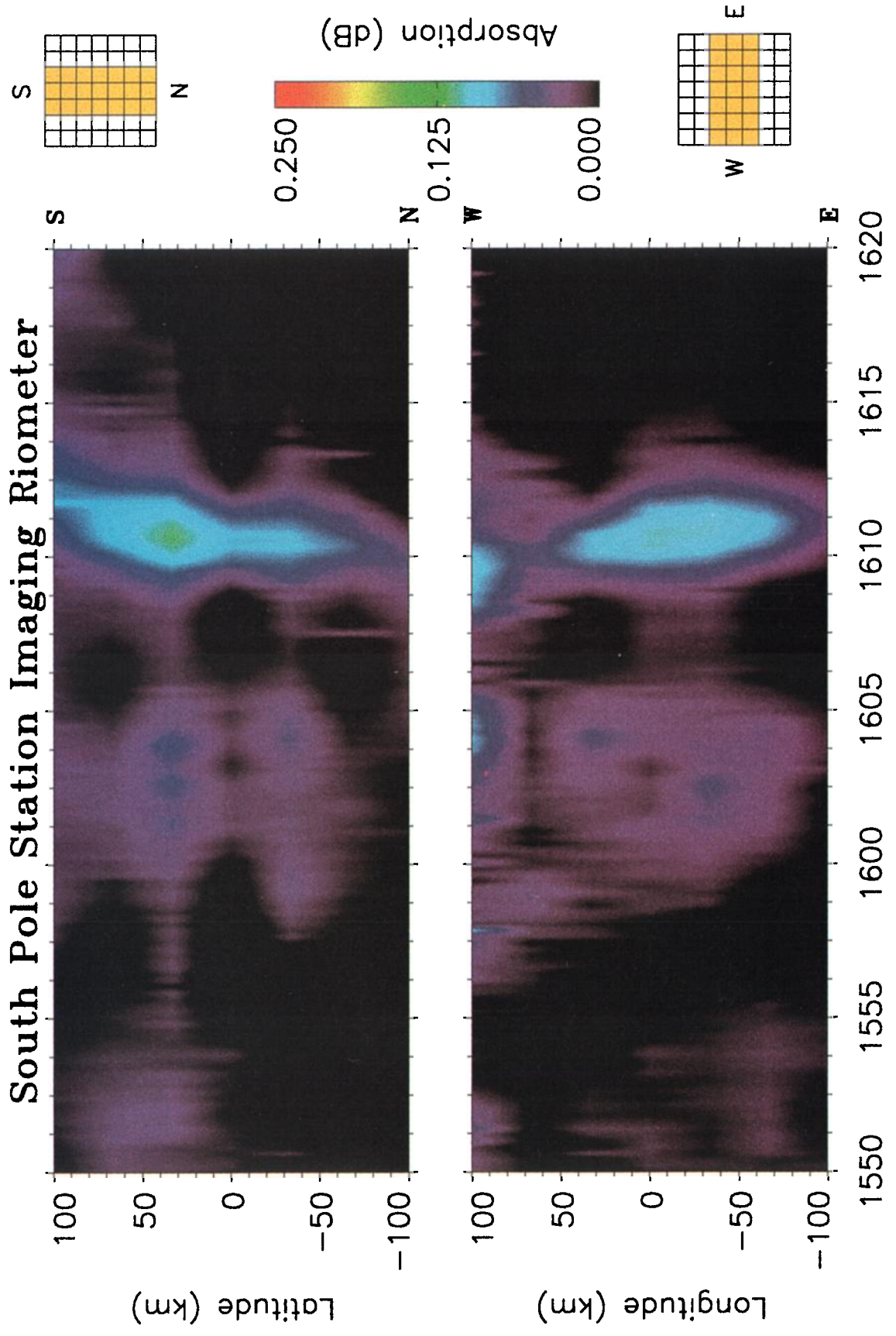

Plate 2. Display of riometer absorption in the geomagnetic (top) south-north and (bottom) east-west directions from the 49-element imaging riometer at SP in the time interval 1550-1620 UT on June 6, 1997.

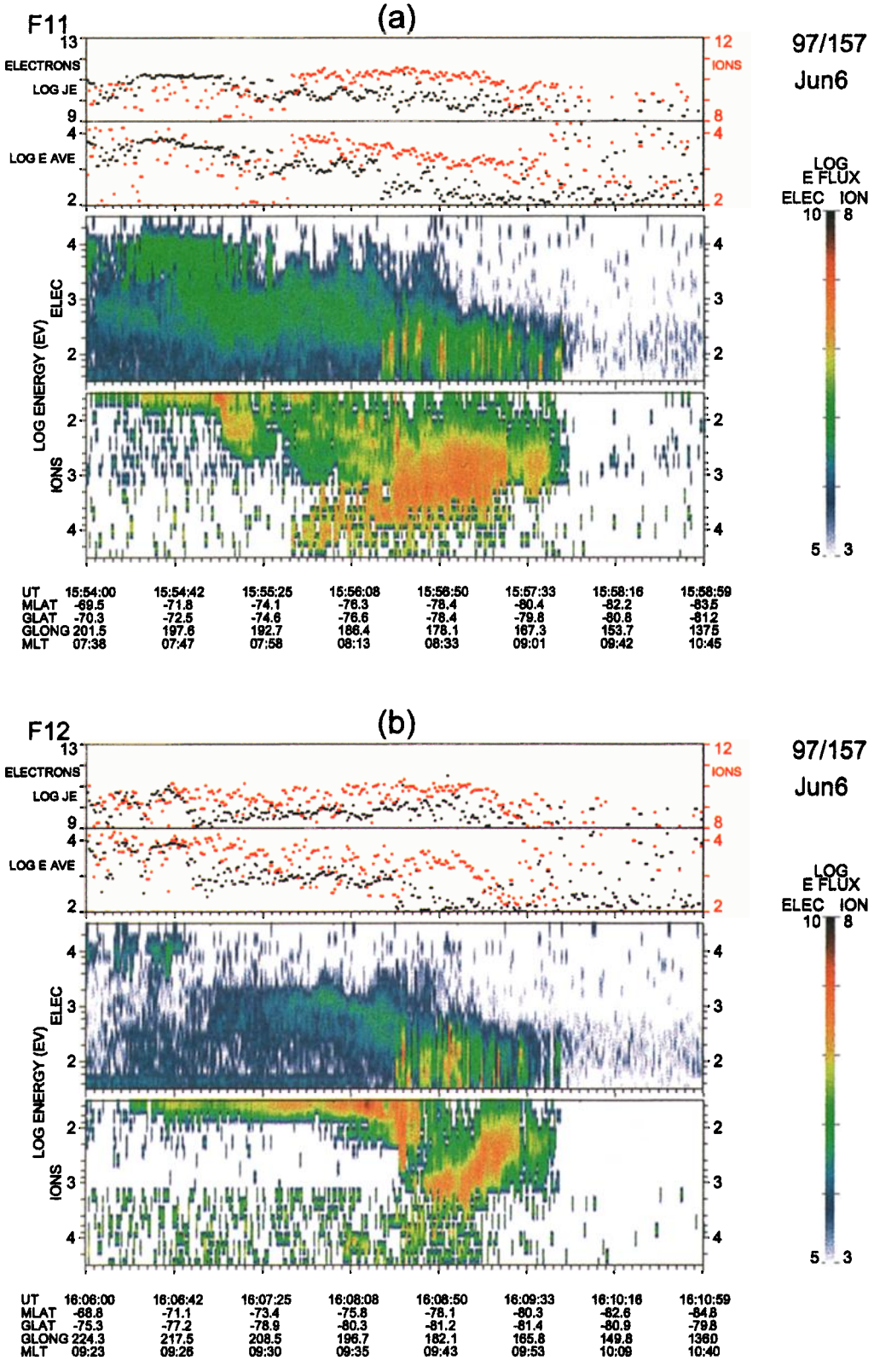

Plate 3. (a) DMSP F11 spectrogram for the interval from 1554 to 1559 UT, and (b) DMSP F12 spectrograms for the interval from 1606 to 1611 UT. (top) Total energy flux in units of eV/(cm2 sec sr) and the average energy (eV) of electrons (black dots) and ions (red dots). The spectrograms show differential energy fluxes of (middle) electrons and (bottom) ions from 32 eV to 30 keV in units of eV/(cm2 sec sr eV).

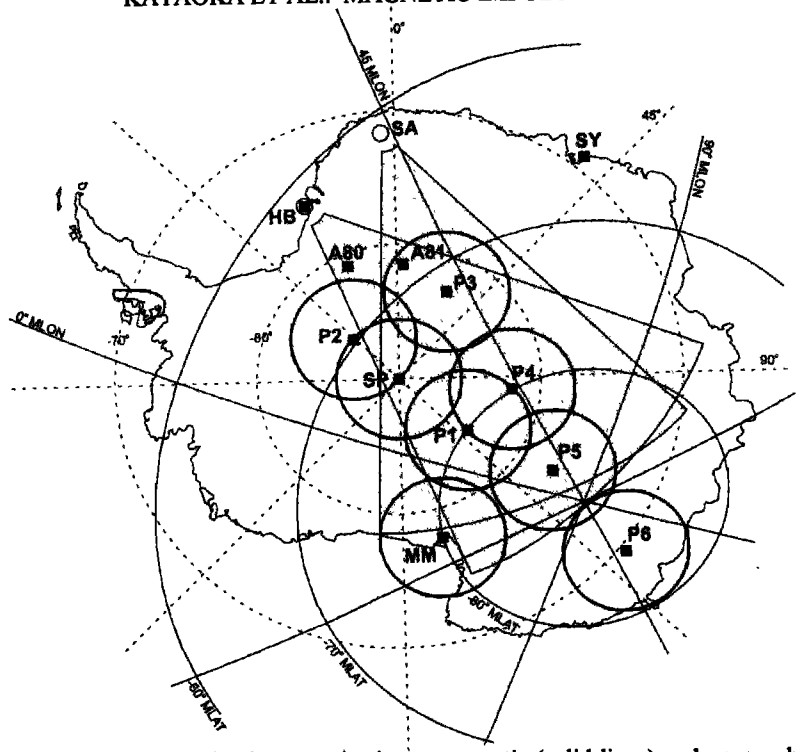

Figure 2. Locations of the Antarctic observatories in geomagnetic (solid lines) and geographic (dashed lines) coordinates. The approximate size of the field of view for optical observation of each station is illustrated assuming that the altitude of the aurora is 200 km, which is typical for 630.0-nm emission. The shaded zone delineates the area covered by HF radars that were used in this study.

3.1. Ground-Based Geomagnetic Data

Throughout this paper, *H*, *D*, and *Z* are used to designate local geomagnetic coordinate directions: *H* for south-north (magnetic field increase northward), *D* for west-east (field increase eastward), and *Z* for vertical (increases in field corresponding to changes downward in the Northern Hemisphere and upward in the Southern Hemisphere). The geomagnetic data from the Antarctic that provided the first evidence of the MIE (Figure 1) were acquired from the two independent sets of automatic geophysical observatories: U.S. AGOs and U.K. AGOs, and three year-round populated stations: SP, McMurdo (MM), and Halley (HB). The locations of the Antarctic observations used in this study are shown in Figure 2 in both geomagnetic (solid lines) and geographic (dashed lines) coordinates. During this event, geomagnetic data from U.S. AGOs P1, P2, and P6 were available. The British AGOs that provided data to the study are identified as A80 and A81. Also shown is the location of the Japanese station at Syowa (SY), whose data were consulted. The intersecting fields of view of HF backscatter radars located at HB and South Africa SANAE station (SA) are indicated. The overall instrumentation and objectives of the U.S. AGO program are provided by *Rosenberg and Doolittle* [1994]. The design, instrumentation, and deployment of the British AGOs are discussed in detail by *Dudeney et al.* [1998].

Geomagnetic data in the hemisphere conjugate to the Antarctic were acquired with wide local time coverage. Four sites associated with the MACCS array (solid squares) in Canada [*Hughes and Engebretson*, 1997], CD, CH, RB, and IG, are illustrated on a geomagnetic (solid lines) and geographic (dotted lines) map in Figure 3. Also shown in Figure 3 are the locations of the Canadian Auroral Network for the OPEN Program Unified Study (CANOPUS) sites (solid triangles), magnetometers of the Danish Meteorological Institute (DMI) in Greenland (solid diamonds), SP conjugate station Iqaluit (IQ) of Bell Laboratories, and the SY conjugate Tjornes (TJ) of the Japanese National Institute for Polar Research (NIPR), whose data have all been used to further illustrate the characteristics of the MIE. The open circles show the corrected geomagnetic (CGM) conjugate points to the Antarctic observatories in order to provide geomagnetic references for the discussions below. The GEO-CGM code provided by the National Space Science Data Center (NSSDC) at Goddard Space Flight Center was used to compute the geomagnetic parameters (http://nssdc.gsfc.nasa.gov/space/cgm/cgm.html).

3.2. Antarctic-Based Optical Data

Optical all-sky imager data were available in the Antarctic at MM, SP, and P1 at the time of the MIE. Unfortunately, cloud cover at P1 prevented good sight during several hours around the MIE. The AGO optical instrumentation is outlined by *Rosenberg and Doolittle* [1994]. The MM data are from instrumentation provided by the University of Newcastle, Australia. At both SP and MM, two wavelengths are recorded simultaneously, 427.8 and 630.0 nm. One image is obtained at 1 min (2 min) intervals at SP (MM).

3.3. Ground-Based Riometer Data

All-sky imaging riometer data were available in the Antarctic at MM, SP, P1, and P2, and at the locations STF and IQ (see Figure 3) in Greenland and Canada, respectively. The Antarctic imaging riometer system has been outlined by *Rosenberg and Doolittle* [1994], while the imaging riometer technique has been described by *Detrick and Rosenberg* [1990].

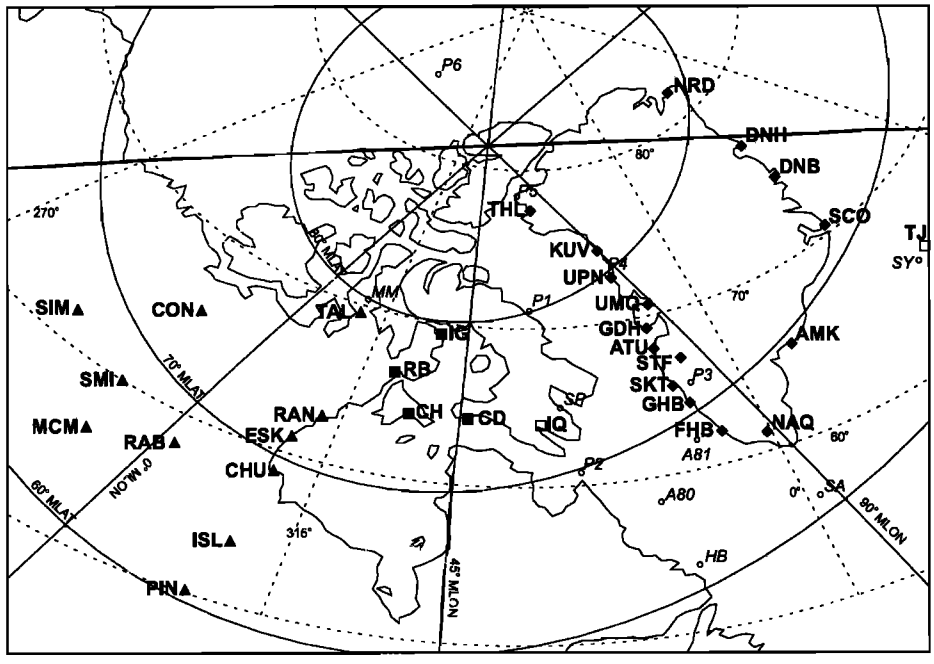

Figure 3. Locations of the Canadian Auroral Network for OPEN Program Unified Study (CANOPUS) (solid triangles), Magnetic Array for Cusp and Cleft Studies (MACCS) (solid squares), and Greenland (solid diamonds) geomagnetic stations used in this study, plotted in both geomagnetic (solid lines) and geographic (dashed lines) coordinates. The CGM conjugate locations for several Antarctic sites are shown as open circles.

3.4. Ground-Based HF Radar Data

The SuperDARN coherent HF radars [*Greenwald et al.*, 1995] are designed to employ backscatter from high-latitude field-aligned ionospheric plasma density irregularities as tracers of the bulk plasma motion under the influence of the convection electric field. During the interval of this MIE, significant backscatter was observed only at the twin radars at SANAE (SA) and Halley (HB) (see Figure 2) in Antarctica.

3.5. Space-Based Data

With the advent of the International Solar Terrestrial Physics (ISTP) program, data from a number of space-based missions are available that can be utilized to investigate the interplanetary conditions that prevailed at the time of the MIE. Interplanetary data from the Wind, IMP8, Interball-Tail, and Geotail spacecraft have been consulted in order to provide information on the interplanetary magnetic field (IMF), solar wind velocity, and plasma number density. The locations of the spacecraft with respect to the locations of the model bow shock [from *Fairfield,* 1971] and magnetopause (from *Roelof and Sibeck* [1993] for solar wind conditions of $B_z = 2.5$ nT and $P =$ 2 nPa) are shown in Figure 4. Data from the low-altitude polar-orbiting DMSP F11 and F12 spacecraft were used to define the high-latitude magnetosphere regions and boundaries prior to and during the MIE. These data, with information on the boundaries as provided by analyses and interpretations of the particle measurements on the DMSP satellites, are available at Johns Hopkins University Applied Physics Laboratory's auroral particles and imagery page (http://sd-www.jhuapl.edu/aurora/index.html).

4. Geomagnetic Data Analysis

4.1. Ground Magnetic Variations

Time-intensity traces of all three components of the magnetic field at the Northern Hemisphere (CANOPUS, MACCS, and Greenland) locations are shown in Figure 5 for the hours 1530-1630 UT, June 6, 1997. All of the data are averaged to 20 s, which is the sampling interval for the Greenland data. The CANOPUS stations are the top 11 traces in Figure 5: the first five traces are the westernmost locations, and the next six CANOPUS traces are the easternmost stations. Each set of CANOPUS locations is plotted in approximately decreasing geomagnetic latitude. The MACCS stations, including IQ, are contained in traces 12-16 from the top, also plotted approximately in decreasing latitude. The west coast of Greenland locations are traces 17-27 from the top (or 7-17 from the bottom), plotted in order of decreasing latitude. The stations on the east coast of Greenland are plotted in order of decreasing latitude in traces 28-32 from the top (or 2-6 from the bottom). The bottom station, TJ, is the conjugate station of SY. The Z component signals in Figure 5 at a number of the Northern Hemisphere stations satisfy the MIE identification criteria established by *Konik et al.* [1994] [see also *Lanzerotti et al.*, 1991]. Large-amplitude (>100 nT), impulsive Z-component signals appear suddenly at ~1610 UT above the much smaller fluctuations of the background geomagnetic field. In general, the MIE signals are also large in the other two components.

4.2. Convection Patterns

Geomagnetic variations were studied in the context of equivalent convection patterns in the ionosphere. To extract the signal of interest, which has a period much shorter than the slow changes of the large-scale ionospheric current system, data values 15 min before and after the specific time are averaged and subtracted from each geomagnetic field component. This is equivalent to high-pass filtering of the magnetometer data with a 30 min frequency cutoff. Two-dimensional convection patterns at 2-min intervals (shown looking down, onto the ionosphere, in both hemispheres) are shown in Figure 6 in CGM coordinates. The

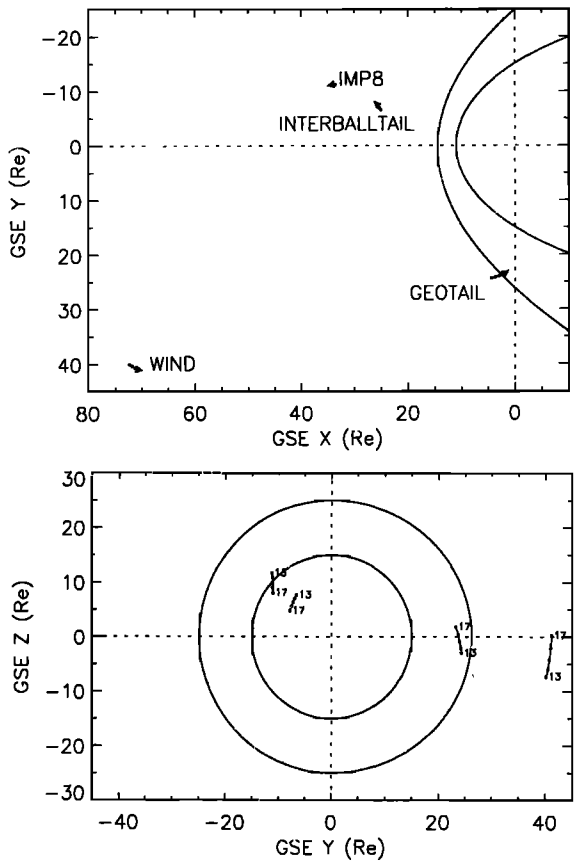

Figure 4. Locations of the spacecraft during the interval 1300-1700 UT on June 6, 1997, showing (top) GSE *Y-X* coordinates and (bottom) GSE *Z-Y* coordinates.

lengths of the convection arrows are expressed in nanoteslas (as that is the unit measured, even though the geomagnetic vectors in the horizontal plane have been rotated by 90° to provide the convection directions) but are proportional to the convection velocities. The vertical component variations at each minute are indicated by the superposed contour. A standard Delaunay triangulation and bilinear interpolation (IDL software package, Research Systems, Inc., Boulder, Colorado, 1995) of the very unevenly distributed data set is performed before making these contour plots. Negative contours are shaded to make them easier to see. The contour interval is 20 nT, and the zero line is removed. Convection patterns are shown at 2-min intervals from 1600 UT to 1616 UT during which the largest amplitude of the MIE was observed.

Beginning at 1602 UT in the Northern Hemisphere and 1604 UT in the Southern Hemisphere, the convection arrows become large enough to indicate a tendency for clockwise rotation in the north and a tendency for counterclockwise rotation in the south. At the same time there is a slight movement of the patterns toward the east (sunward) in both hemispheres. The TCV patterns with more than 1000 km extent in the longitudinal direction crossed magnetic noon at ~1606 UT and decayed around 14 MLT at ~1612 UT. The vertical component in the TCV is negative in both hemispheres: over the MACCS stations and the southern stations (as is also shown in Figure 5). This negative *Z* component, together with the clockwise rotations in the north and counterclockwise rotations in the south, is consistent with field-aligned currents out of the ionosphere in both hemispheres [e.g., *Lanzerotti et al.*, 1991].

5. Aurora and CNA Data Analysis

Available optical data acquired in the Antarctic near the dayside auroral oval were investigated. Optical data (630.0 and 427.8 nm) were available from MM (Arrival Heights installation by the University of Newcastle, Australia) and at SP. Unfortunately, the atmosphere over the only operating AGO all-sky imager at P1 was clouded out. Shown in Plate 1 are 630.0-nm all-sky images from MM and SP in geomagnetic coordinates for the interval 1556 UT (top left) to 1624 UT (bottom right). The images are shown at 2-min intervals from top to bottom and left to right.

An aurora aligned in the geomagnetic east-west direction was observed in the MM image at 1556 UT. This aurora began to move westward at 1558 UT. The auroral intensity suddenly increased at the MIE onset at 1600 UT, and then the aurora split at 1602 UT. A portion of the aurora moved westward (see MM image at 1604 UT), while the eastern portion moved eastward and disappeared from the MM image at 1606 UT. At SP the image showed auroral brightening after 1606 UT. This aurora moved eastward with a speed of 1-3 km/s until the aurora became diffuse at 1614 UT. In the SP image at 1616 UT an arc structure aligned in the longitudinal direction detached from the bulk of the aurora and moved equatorward. The formation of the arc structure is more evident in background subtracted images (not shown here). The auroral arc halted at ~74° MLAT and brightened at 1619 UT (not shown here) and then decayed. Considering the morphological picture of dayside precipitation boundaries of *Newell and Meng* [1992] near magnetic noon, the discrete arc may indicate that the MIE is related to the low-latitude boundary layer rather than to the boundary plasma sheet. There was little signal at 427.8 nm at either of these sites. The dominant 630.0-nm emission indicates the precipitation of primarily low-energy electrons.

The precipitation of primarily low-energy electrons is further confirmed by an investigation of the imaging riometer data from MM, P1, P2, and SP. If there is a sufficient flux of higher-energy electron precipitation, the D region ionization will be enhanced, and this will produce cosmic noise absorption (CNA) in riometer signals. There was no significant CNA measured at MM, P1, or P2 during the MIE. Data obtained from the imaging riometer at SP are shown in Plate 2. Only very weak absorption is observed, but the signal clearly exhibits eastward and sunward motion starting at 1609 UT. This movement is essentially consistent with the movement of the 630.0-nm emissions seen in Plate 1.

6. HF Radar Analysis

The SuperDARN radars observed almost no backscatter corresponding to this event in either the Northern Hemisphere or the Southern Hemisphere. The exception was a preexisting stable region of irregularity that is depicted in a grayscale area in Figure 7, in which the spectral power of backscatter observed by the SANAE radar at 2-min intervals is shown. The gray-scale area is mapped onto the 300-km altitude (a typical altitude for *F* region backscatter). Circles are the fields of view of the all-sky imagers (same as Plate 1) and are shown as a guide for the relative locations. Preexisting radar scatter was also seen in the Halley radar field of view. The backscatter power in the preexisting HF radar scatter region was enhanced when the TCV approached the backscatter region and passed through it, suggesting that the TCV current system caused an intensification of the ionospheric irregularities. At 1614 UT, when the MIE-related aurora reached the backscatter region,

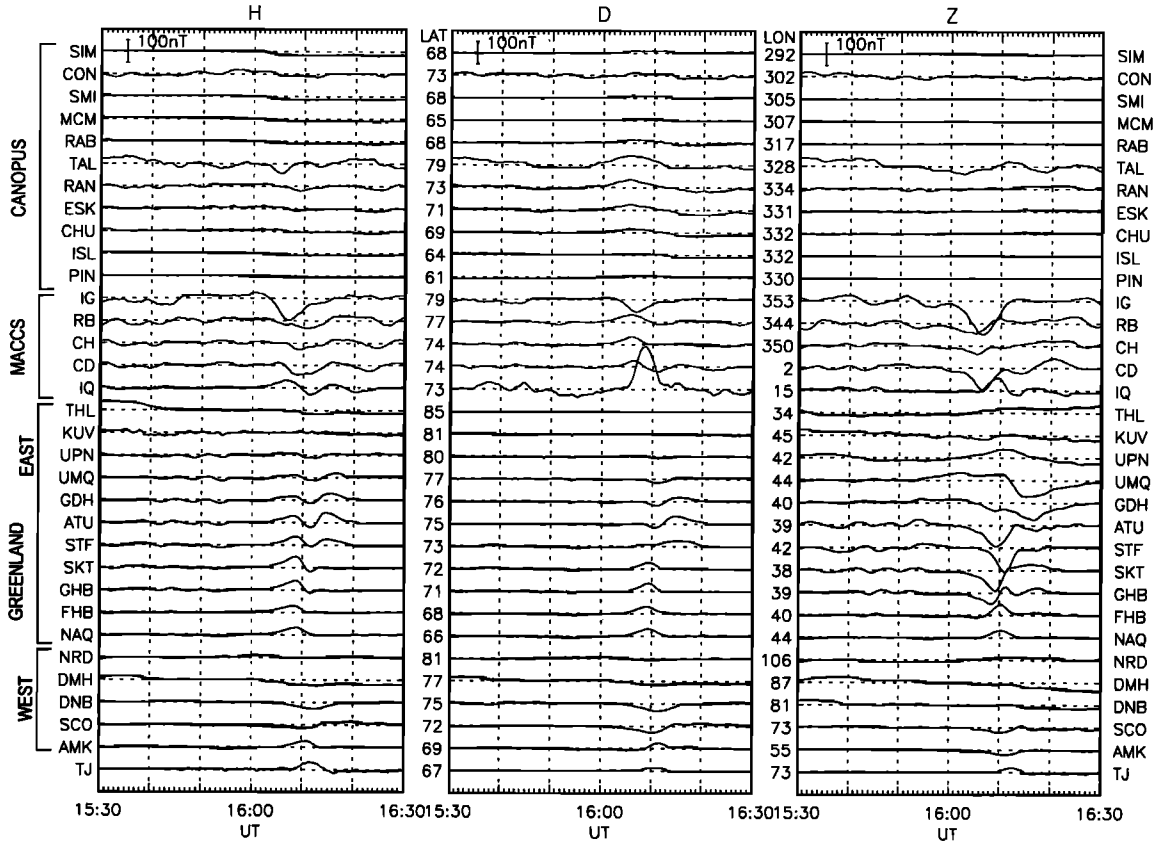

Figure 5. Time-intensity traces for all three magnetic field components measured at Northern Hemisphere magnetometer locations for the hour interval (1530-1630 UT) around the time of the MIE on June 6, 1997.

the peak power was measured at the western edge of the backscatter region. The enhancement of the irregularities gradually faded out, lasting until ~1700 UT. The Halley radar also observed a backscatter intensification similar to that of the SANAE radar.

The twin radar data also show a very pronounced increase in the Doppler spectral width (the full width of the Doppler spectra at half power) as the vortex passes through the irregularity region (not shown). The Doppler spectral width is a measure of the variation of the electric field in both the spatial domain (the radar sampling cell, typically 45 km by 100 km in dimension) and the time domain (variations occurring during the radar integration time, which was 7 s). A large increase in the spectral width indicates that the electric field has varied rapidly in one or both of these two domains. *André et al.* [1999, 2000] have evaluated the impact of a time-varying electric field on the spectral width.

The convection patterns derived from the radar data for the time interval 1602 to 1630 UT at 2-min intervals are shown in Figure 8. The two-dimensional convection velocities are calculated by the vector addition of two line-of-sight Doppler velocities in the overlapped backscatter region. A strict threshold is used in order to provide reliable vector velocities: The minimum power and velocity thresholds are 3.0 dB and 25 m/s, respectively, while the maximum velocity and its error are 3000 and 100 m/sec, respectively.

The convection velocities in Figure 8 show that the characteristic change of the convection velocity began at ~1606 UT. No merged vectors were available in the field of view for the previous two panels at 1602 UT and 1604 UT. The plasma flows show a rotation similar to the convection arrows at SP in Figure 6. However, there is ~2-min time lag between the SP geomagnetic signature and the HF radar signature. The convection arrows obtained from the HF radar data are located ~2° equatorward and 10-15° eastward of SP station. The merged region moved eastward across the ~30° geomagnetic meridian. The convection velocity increased to ~2400 m/s at 1612 UT. All of these signatures are consistent with the passage of the low-latitude portion of the TCV.

7. Interplanetary Conditions

Shown in Figure 9 are the solar wind velocity, dynamic pressure, and interplanetary magnetic field (IMF) in GSM coordinates as measured on IMP8 (see Figure 4) for the interval, 1300-1700 UT around the MIE. The magnetic field data and its variations as measured on Interball-Tail are also shown in Figure 9 by dotted lines. The IMF values are ~1-min values for IMP8 and 2-min averages for Interball-Tail. The solar wind data in the bottom three panels are displayed at ~90-s resolution. The locations of IMP8 and Interball-Tail were GSE (x, y, z) = (34.2, -10.9, 10.0) and GSE (x, y, z) = (25.6, -7.2, 6.4) at 1510 UT, respectively.

There are several ways to estimate the time for an interplanetary magnetic feature to propagate from the position of a satellite to the bow shock or the magnetopause. The most straightforward estimate is to assume that the magnetic feature is contained in a plane oriented parallel to the y-axis. Using the

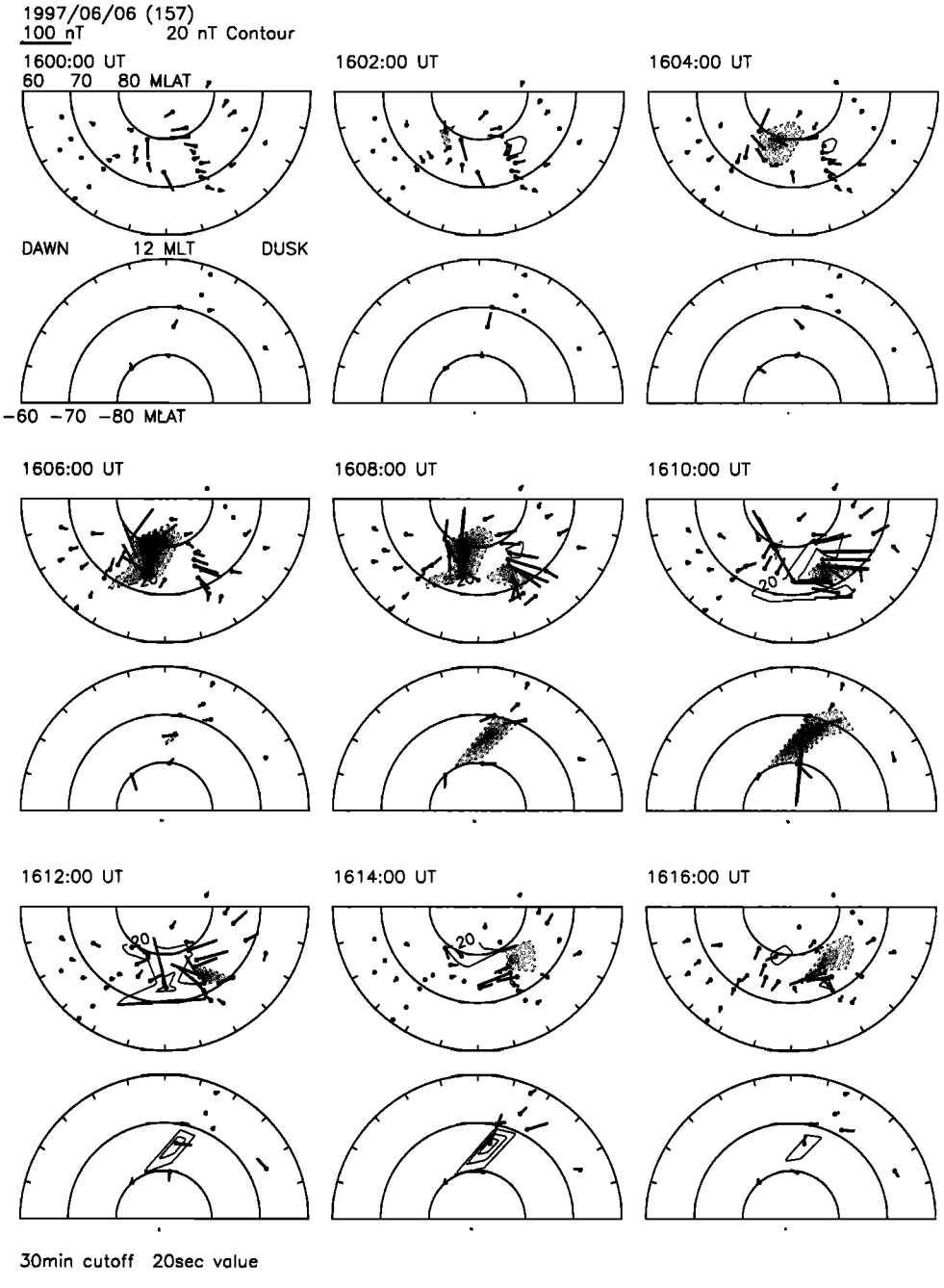

Figure 6. Equivalent convection plots for all magnetometer stations at 2-min intervals beginning at 1600 UT. A pair of downward and upward semicircles show the patterns for the Northern and Southern Hemispheres, respectively. The magnitude and direction of change of the Z component are also plotted by superposed contour.

solar wind velocity and the spacecraft x position, a simple estimate of the propagation time can be determined. Assuming that the subsolar bow shock and magnetopause are located at 14.5 and 11.0 R_E, respectively, as depicted in Figure 4, and the solar wind velocity V_{sw} is 400 km/s, this estimation results in a delay of 13 min from IMP8 to the subsolar magnetopause and a delay of 11 min from Interball-Tail to the magnetopause (here we assume that the propagation velocity in the magnetosheath $V_{sh} = V_{sw}/8$). Note that this implies that the propagation time from IMP8 to Interball-Tail is ~2 min, a time somewhat shorter than the observed time delay in Figure 9. Therefore this simple estimation method could be improved.

The above method is not valid when the spacecraft are substantially off the Sun-Earth line and the orientation of the interplanetary structure is not perpendicular to the solar wind flow direction. For this MIE, since the vector from IMP8 to Interball-Tail points toward the nose of the bow shock and two satellites observed almost identical signatures, we can estimate the propagation time from the spacecraft to the bow shock more accurately. There are two distinguishable discontinuities that might possibly trigger the MIE, i.e., a large cone angle change at 1508 UT and a rapid southward turning at 1516 UT on IMP8.

Since the observed time lag between IMP8 and Interball-Tail is ~7 min for the cone angle change, it would take ~9 min to

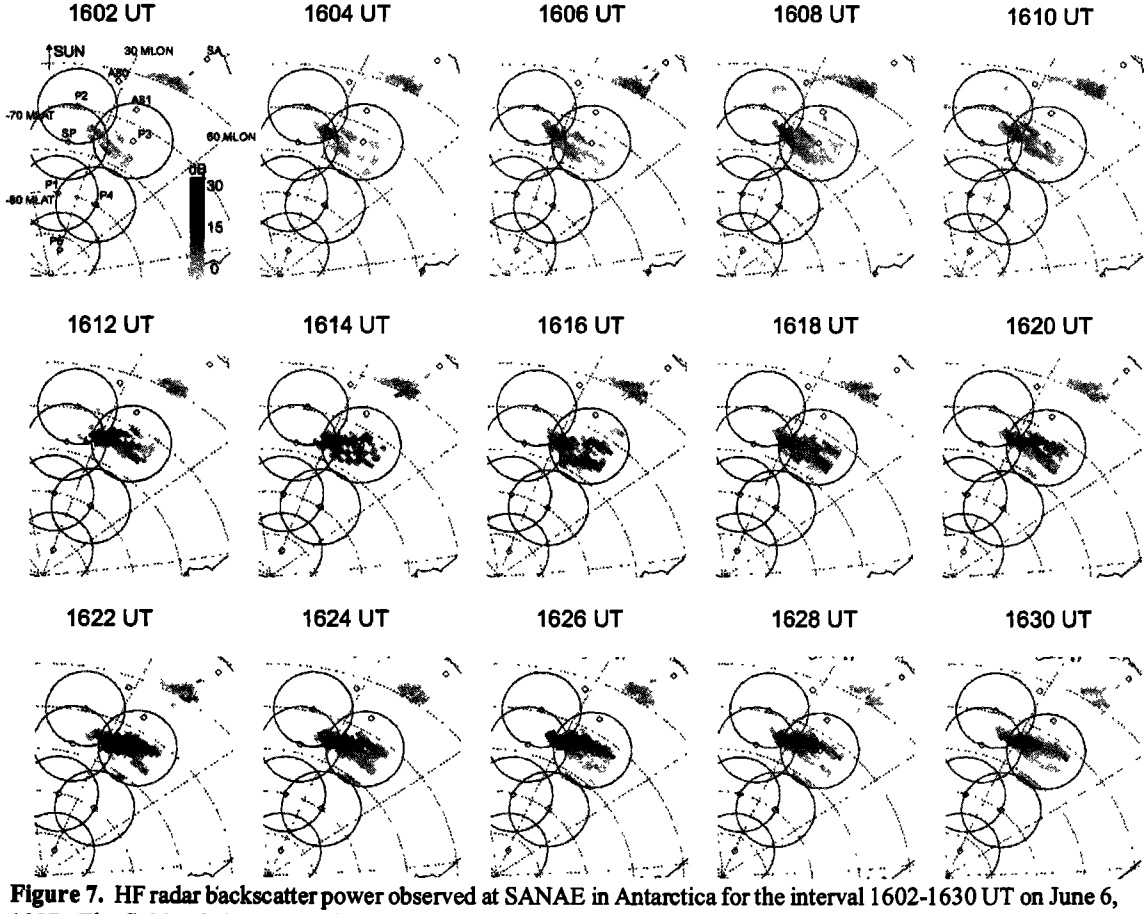

Figure 7. HF radar backscatter power observed at SANAE in Antarctica for the interval 1602-1630 UT on June 6, 1997. The fields of view of all-sky cameras are also depicted.

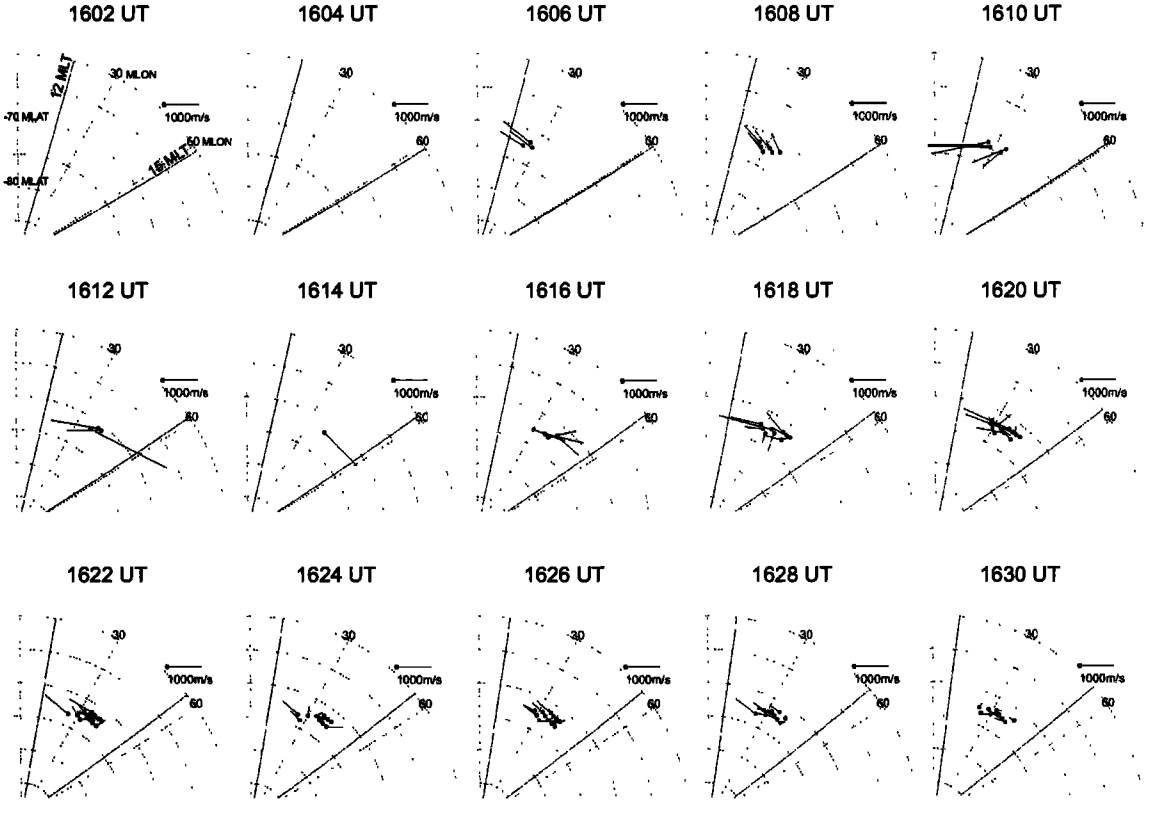

Figure 8. Two-dimensional convection velocities derived from the merging method of line-of-sight Doppler velocities observed by twin radars, SANAE and Halley, for the interval from 1602 UT to 1630 UT on June 6, 1997.

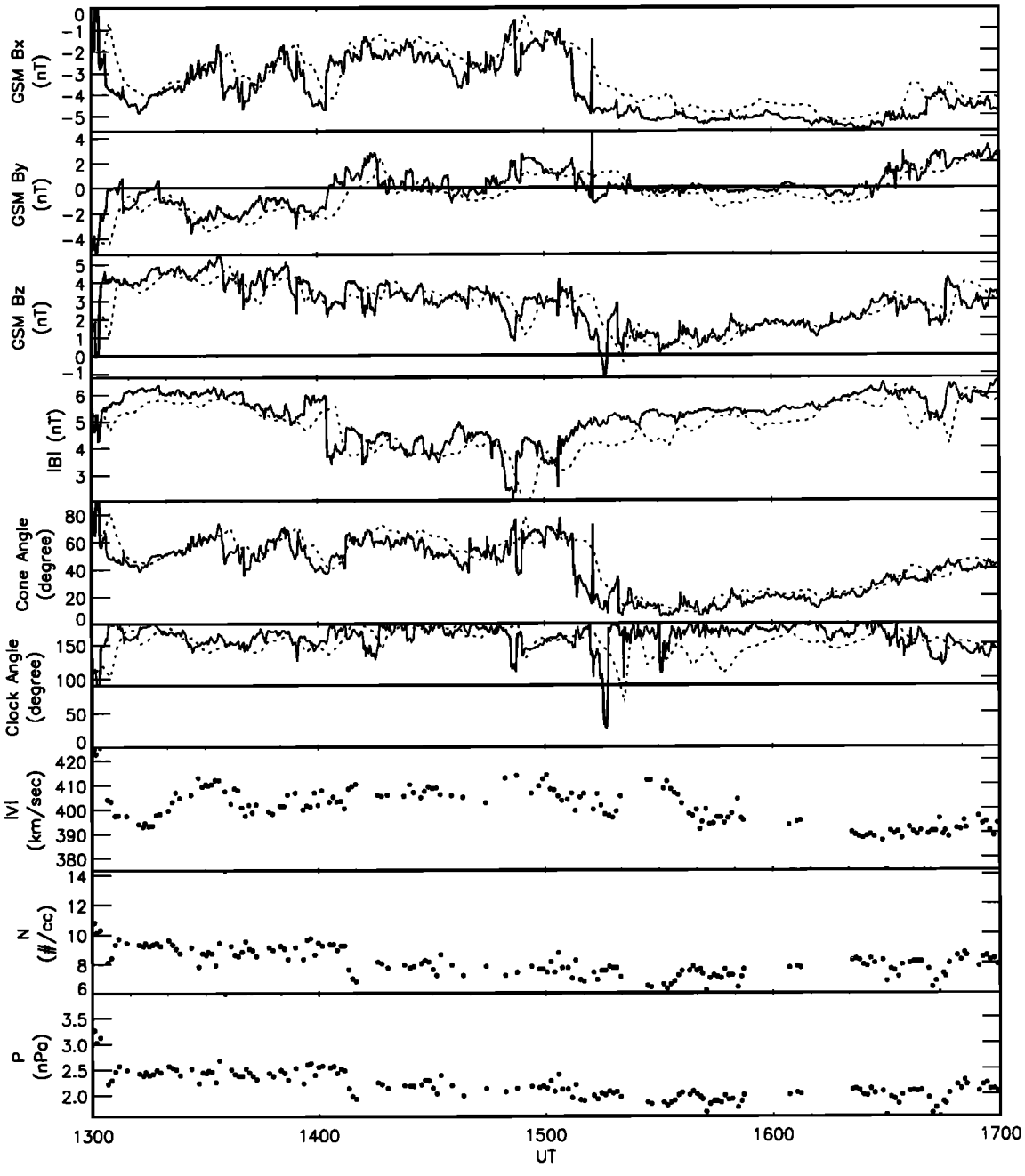

Figure 9. Interplanetary data from the IMP8 and Interball-Tail spacecraft for the interval 1300-1700 UT on June 6, 1997. (top to bottom) Interplanetary magnetic field (IMF) B_x, B_y, and B_z component magnitudes (in nanoteslas and GSM coordinates); total field strength B (nT); cone angle and clock angle of IMF (in degrees); the solar wind speed $|V|$ (km/s); ion number density n (cm^{-3}); and dynamic pressure P (nPa). The Interball-Tail magnetic field data are shown by dotted lines in the top six panels.

propagate from Interball-Tail to GSE $(x, y, z) = (15.0, -2.6, 2.0)$, near the nose of the bow shock along the line from IMP8 to Interball-Tail. In the same way, since the observed time lag between IMP8 and Interball-Tail is ~5 min for the southward turning, it would take ~6 min propagation time from Interball-Tail to the point GSE $(x, y, z) = (15.0, -2.6, 2.0)$. If the transmission time from the bow shock to the magnetopause is taken to be ~6 min, these discontinuities should reach the vicinity of the magnetopause nose between 1530 UT and 1533 UT. Thus we can conclude that these discontinuities are not the direct trigger of the beginning of the MIE at ~1600 UT.

During the time interval after the passing of these two discontinuities (including the MIE interval), the IMF had a large X component (~-4 to -5 nT); almost zero Y component; and a small, positive Z component. Thus the IMF was nearly radially aligned during this time, with a cone angle of <20° (see the fifth panel from the top in Figure 9). There were only small fluctuations in the solar wind velocity (which was low, ~400 km/s) and in the dynamic pressure throughout the 4-hour interval shown in Figure 9. Although we have also examined data from the Wind and Geotail satellites, these data are not shown here, because the two satellites are located on the far

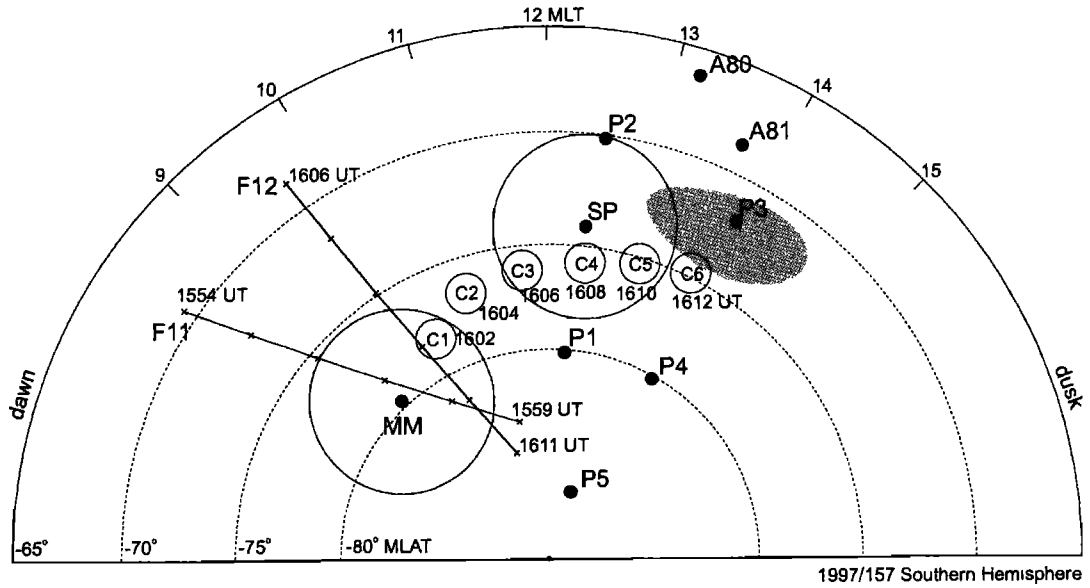

Figure 10. Schematic illustration of the MIE occurrence region and its movement on the geomagnetic polar map. The guiding centers of the traveling convection vortex (TCV) derived from the horizontal perturbations are plotted as C1 to C6. Shaded area indicates the backscatter region observed by the Super Dual Auroral Radar Network (SuperDARN) radars in Antarctica. The tracks of DMSP F11 and F12 spacecraft across the Southern Hemisphere at the beginning and end of the MIE are also depicted.

duskside away from the Sun-Earth line, which is not relevant to the discussion of the MIE triggering. In summary, the data obtained from the IMP8 and Interball-Tail spacecraft do not show solar wind signatures that would lead to the conclusion of a direct triggering of the MIE.

8. Discussion

The previous sections have presented ground signatures of the MIE on June 6, 1997, using observations of geomagnetic variations, aurora, particle precipitation, cosmic noise absorption, and HF radar backscatter. A summary of the direction of motion of the MIE is shown in Figure 10 on a polar map of the Southern Hemisphere. The symbols C1 to C6 in Figure 10 are the approximate guiding centers of the MIE (TCV) at 2-min intervals from 1602 to 1612 UT. The approximate location of each center is inferred from the equivalent convection arrows in Figure 6. Although this method for the determination of the center of the MIE may not be as rigorous as using a model, we are simply interested in examining and comparing the gross features for the motion of the vortex. In this manner the center is, at first, determined for the northern vortex; the center is then projected to the CGM conjugate points in the Southern Hemisphere. Since these conjugate points are also consistent with the location of the vortex observed in the Southern Hemisphere, it is concluded that there is a good conjugacy in CGM coordinates in terms of the guiding center of the vortex. The MIE was initiated at C1 in the prenoon local time region in both hemispheres as shown in Figure 10. The optical data in the Antarctic, as well as the geomagnetic data, show that the MIE then moved eastward (noonward) and equatorward from C1 to C6 across the magnetic local noon meridian.

The scale size and motion of the MIE/TCV can be further delineated by examining the timing and the amplitude of the vertical (Z) component observed in both hemispheres. The MIE had its earliest (~1607 UT), and approximately largest, Z component amplitude (~150 nT) at IG (see Figure 5). A minute or two prior to this there was a small vertical deflection at MM (see Figure 1). Vertical variations were seen at almost the same time at RB and CH of the MACCS array. In the CANOPUS magnetometer chain located west of the MACCS array, there were no vertical variations; D component variations that might be associated with the MIE were seen at the four most northern and eastern CANOPUS locations, CHU, ESK, RAN, and TAL. Two minutes after the event at the western edge of the MACCS array, the largest vertical components were seen over SP at ~1609 UT in the Antarctic and at ATU and SKT on the western edge of Greenland. About 1 to 2 min later (~1611 UT), a large Z amplitude was seen over STF with riometer absorption in the region equatorward of STF. The MIE basically ended at about this time (~1612 UT). Thus the overall timing of the largest amplitude in the Z component intensities followed, ~1-3 min behind, the timing of the guiding center motion that is depicted in Figure 10.

The motion and the current system of the MIE can be described overall by making reference to the all-sky imager, imaging riometer, and HF radar data. A 630.0-nm auroral brightening at 1600 UT at -78° MLAT and subsequent splitting into the western and eastern portions (see a clear gap in the auroral image from MM at 1606 UT in Plate 1) were observed in the prenoon sector (~10 MLT), and the eastward moving aurora decayed at -75° MLAT in the afternoon sector (~14 MLT). At 1608 UT, when the center of the MIE was located near location C4, the peak luminosity of the MIE-related 630.0-nm aurora was observed around location C3. At 1610 UT the all-sky imager at SP observed the brightest aurora just poleward of SP near C4, while the center of the vortex was located at C5 at this time. This 2-min time lag, as well as the 1- to 3-min time delay of the Z component response to the guiding center, may indicate that the upward field-aligned current was located near the rear edge of the Hall current loop rather than at the center of the loop.

The imaging riometer at SP observed weak CNA associated with this MIE. The eastward motion is clear in Plate 2. The indicated motion nearly corresponds to the motion of the

630.0-nm aurora. While the absorption level is very low (< 0.13 dB), it is larger than the noise level (~0.05 dB) of the instrument. In the polar region most riometer measurements are dominated by *D* region absorption arising from energetic particle precipitation. However, the CNA event in this paper cannot be considered as a result of hard electron precipitation, because there was no blue aurora at 427.8 nm at SP, which would be caused by hard electron precipitation. A weak CNA event without hard electron precipitation can be interpreted by two mechanisms: either enhanced ionization in *F* region patches [cf. *Rosenberg et al.*, 1993] or heating of electron temperatures in the *E* region [cf. *Stauning*, 1984]. The *F* region ionization scenario may be consistent with the 630.0-nm optical observations, which show an enhancement at the time of the MIE. The 630.0 nm-aurora is usually emitted at *F* region altitudes. On the other hand, *E* region heating may also contribute to this CNA event. The *E* region heating explanation argues for a cause by a localized, strong increase of the horizontal electric field. Further quantitative analysis is needed to understand this weak CNA event.

Particle data from the low-altitude DMSP spacecraft passing over the polar regions were examined to determine the locations of various high-latitude features. During the time closest to the MIE, most passes were over the Southern Hemisphere and are therefore most relevant to this discussion. In particular, the passes of DMSP F11 and F12 over the Antarctic are the closest ones in time to the MIE. Plate 3a shows that DMSP F11 observed LLBL precipitation from -77° to -80° MLAT as it passed over the 630.0-nm aurora seen in the MM image in the interval of 1557 to 1558 UT. Since the particle signature does not have a clear LLBL/mantle boundary, the precise poleward boundary of the LLBL cannot be specified. However, considering the drop-off of the highest-energy ions and a sharp drop in the ion fluxes at lower energies (although they briefly recovered), the boundary is possibly at ~80° MLAT. The ion and electron energies and the flux intensities in the region above ~80° MLAT are consistent with the characteristics of the mantle. The 630.0-nm optical data from MM (see Plate 1) also show a sharp boundary of the emissions at ~80° MLAT.

DMSP F12 (see Plate 3b) encountered a clear mantle/LLBL boundary, i.e., an open/closed boundary, at ~79° MLAT and 9.7 MLT at 1609:30 UT. It is apparent from Plate 1 that this open/closed boundary also corresponds to the poleward boundary of the 630.0-nm aurora. In actuality, the auroral emission region moved slightly equatorward as the event moved eastward. From the discussion above and Figure 10, it is concluded that the MIE was initiated in the LLBL.

Investigation of the conditions in the interplanetary medium both near Earth as well as farther upstream shows that there were no significant changes in the solar wind dynamic pressure at the time corresponding to the onset of the event. The IMF was directed strongly radially outward from the Sun and had a slightly positive (~1-2 nT) northward orientation in the GSM coordinates. There are significant pieces of evidence against the classical explanations of MIE initiation, such as dayside reconnection, pressure pulse, impulsive plasma penetration, and Kelvin-Helmholtz instability. For example, the positive IMF B_z condition would tend to exclude dayside reconnection. The eastward (toward dusk) motion of a MIE across the magnetic noon meridian is clearly opposite to the predicted propagation direction from impulsive plasma penetration or Kelvin-Helmholtz instability. The pressure pulse mechanism is excluded by the absence of abrupt solar wind dynamic pressure changes. The configuration of the IMF could potentially lead to some high-latitude reconnection, which would probably have significantly different signatures in the two polar regions [e.g., *Lockwood and Moen*, 1999]. It still seems difficult to explain the observed conjugacy of the TCV structure only by such a high-latitude reconnection model.

The interaction between the bow shock and the solar wind may provide a trigger source for the MIE. The nearly radial direction of the IMF at the time of occurrence of the MIE produces a quasi-parallel shock (QPS) structure at the bow shock. It is known that during QPS conditions the magnetosheath exhibits a disturbed state [e.g., *Schwartz and Burgess*, 1991]. Rapid pressure variations could exist in the magnetosheath at this time. The strong Pc3 geomagnetic activity that was observed during the MIE interval (not shown) may also be related to the QPS condition. However, even if such pressure variations did stimulate this MIE, critical questions still remain: Were they of sufficient amplitude to produce such a MIE? How could such pressure variations produce the sunward motion of the TCV accompanied by the MIE? How are the clearly impulsive and nonturbulent characteristics of the MIE phenomena produced under the influence of turbulent conditions? It appears that no present models can readily explain all of the MIE features of this event in a unified fashion. There are abrupt IMF cone angle changes from 60° to 20° observed at 1508 and 1515 UT at IMP8 and Interball-Tail, respectively. Via the cone angle change, the foreshock region will expand into a large area. The expansion direction will be from dawn to dusk, which is consistent with the propagation direction of the MIE. Although the cone angle change occurs ~30 min prior to the MIE onset, it is speculated at this time that the rapid change of the foreshock geometry has been the indirect trigger of the MIE on June 6, 1997.

9. Conclusion

A magnetic impulse event on June 6, 1997, was investigated using an extensive, multi-instrument data set. The result of a conjugate hemisphere analysis using magnetometer network data in northern and southern high-latitude regions was reported for the first time in this paper. Simultaneous auroral, CNA, and HF backscatter data were also analyzed to investigate the further motion of a traveling convection vortex accompanying by the MIE. The analysis demonstrated that it was worthwhile to use the vertical component of the MIE-perturbed magnetic field to trace the TCV motion, despite possible induction effects. The main results are summarized as follows.

1. A TCV related to the MIE on June 6, 1997, was initiated at ~10 MLT and ~78° MLAT in the LLBL. The motion of the TCV was eastward (toward dusk) and slightly equatorward across the magnetic noon meridian, with a traveling velocity of 1-3 km/s at Earth's surface. The TCV has conjugate guiding centers in the northern and southern hemisphere.

2. All-sky cameras observed the 630.0-nm aurora following the motion of the TCV guiding center with an ~2-min time delay. It was found that the upward field-aligned current was located near the rear edge of the Hall current loop rather than at the center of the loop. The imaging riometer only at SP observed a weak cosmic noise absorption event and similar eastward motion. This MIE-related CNA may imply *F* region electron density enhancement by localized soft electron precipitation.

3. There were no abrupt changes in the solar wind dynamic pressure or interplanetary magnetic field that could be the direct trigger of the MIE. The IMF showed strongly outward (-5 nT) B_x, slightly positive (1-2 nT) B_z, and nearly zero B_y orientation in GSM coordinates. The classical generation mechanisms of MIEs such as dayside reconnection, pressure pulse, Kelvin-Helmholtz instability, and plasma penetration are excluded as candidate mechanisms for this MIE. Although the origin of this MIE is not clear, it is speculated that a possible indirect trigger may be the abrupt IMF cone angle change from 60° to 20°, ~30 min ahead the onset, via the interaction between the solar wind and the bow shock.

Acknowledgments. We express our sincere thanks to all members of the geomagnetic field observation network teams: the Greenland chain, the CANOPUS, and the MACCS. We thank L. V. Medford of Bell Laboratories for his capable engineering assistance with the magnetometers in the Antarctic. We deeply appreciate the assistance of J. Watermann with handling the data from the Greenland magnetometer chain, which is operated by the Danish Meteorological Institute. Also, thanks are extended to T. Hughes for magnetometer data from CANOPUS. The CANOPUS instrument array was constructed, maintained, and operated by the Canadian Space Agency for the Canadian scientific community. We also thank M. Engebretson (Augsburg College) for use of magnetometer data from MACCS. The Halley and U.K. AGO magnetometer data were provided by the British Antarctic Survey (BAS) of the Natural Environmental Research Council (NERC), Cambridge, U.K. We acknowledge N. Sato, National Institute of Polar Research (NIPR), Japan, for providing magnetometer data from Syowa and Tjornes stations and for SuperDARN data. The SHARE HF radar at SANAE Station, Antarctica (principal investigator (PI), A.D.M. Walker, University of Durban) was developed under funding from the South African Department of Environmental Affairs and Tourism (DEAT), the U.K. NERC, and the U.S. National Science Foundation (NSF) (grant OPP-9421266). Operations are supported by DEAT. The Halley radar (PI, M. Pinnock, British Antarctic Survey) was developed under funding from the U.K. NERC and the U.S. NSF (grant DPP-8602975). Operations are funded by the U.K. NERC. We sincerely thank B. J. Fraser and I. Wright for the use of all-sky imager data at Arrival Heights (MM). The instrument is operated by the Space Physics Group and Cooperative Research Centre for Satellite Systems, University of Newcastle, Australia. Also, we acknowledge P. Newell (Johns Hopkins University Applied Physics Laboratory) for his comments on particle precipitation and for use of the DMSP particle data. The DMSP SSJ/4 particle detectors were built and calibrated by D. Hardy and F. Rich of the Air Force Research Laboratory. We also thank the very helpful system of the NASA NSSDC ISTP program (CDAWeb, SpyCAT, SSCWeb) and related PIs for allowing the browsing of useful key parameter data from many satellites consulted in this paper.

Janet G. Luhmann thanks John R. Dudeney and Therese Moretto for their assistance in evaluating this paper.

References

André, R., M. Pinnock, and A. S. Rodger, On the SuperDARN autocorrelation function observed in the ionospheric cusp, *Geophys. Res. Lett., 26*, 3353, 1999.

André, R., M. Pinnock, and A. S. Rodger, Identification of low-altitude cusp by Super Dual Auroral Radar Network radars: A physical explanation for the empirically derived signature, *J. Geophys. Res, 105*, 27081, 2000.

Bering E. A., L. J. Lanzerotti, J. R. Benbrook, Z.-M. Lin, C. G. Maclennan, A. Wolfe, R. E. Lopez, and E. Friis-Christensen, Solar wind properties observed during high-latitude impulsive perturbation events, *Geophys. Res. Lett., 17*, 579, 1990.

Detrick, D. L., and T. J. Rosenberg, A phased-array radiowave imager for studies of cosmic noise absorption, *Radio Sci., 25*, 325, 1990.

Dudeney, J. R., R. I. Kressman, and A. S. Rodger, Automated observatories for geospace research in polar regions, *Antarct. Sci., 10*, 192,1998.

Dungey, J. W., Interplanetary magnetic field and the auroral zone, *Phys. Rev. Lett., 6*, 47, 1961.

Fairfield, D. H., Average and unusual locations of the Earth's magnetopause and bow shock, *J. Geophys. Res., 76*, 6700, 1971.

Farrugia, C. J., M. P. Freeman, S. W. H. Cowley, D. J. Southwood, M. Lockwood, and A. Etemadi, Pressure-driven magnetopause motions and attendant response on the ground, *Planet. Space Sci., 37*, 589, 1989.

Friis-Christensen, E., M. A. McHenry, C. R. Clauer, and S. Vennerstrom, Ionospheric traveling convection vortices observed near the polar cleft: A triggered response to sudden changes in the solar wind, *Geophys. Res. Lett., 15*, 253, 1988.

Fukunishi, H., and L. J. Lanzerotti, Hydromagnetic waves in the dayside cusp region and ground signatures of flux transfer events, in *Plasma waves and Instabilities at Comets and in Magnetospheres, Geophys. Monogr. Ser.*, vol. 53, p. 179, edited by B. Tsurutani and H. Oya, AGU, Washington, D. C., 1989.

Fukushima, N., Equivalence in ground geomagnetic effect of Chapman-Vestine's and Birkeland-Alfven's electric current-systems for polar magnetic storms, *Rep. Ionos. Space Res. Jpn. 23*(3), 219, 1969.

Glassmeier, K.-H., M. Hönisch, and J. Untiedt, Ground-based and satellite observations of traveling magnetospheric convection twin vortices, *J. Geophys. Res., 94*, 2520, 1989.

Glassmeier, K.-H., and C. Heppner, Traveling magnetospheric convection twin vortices: Another case study, global characteristics, and a model, *J. Geophys. Res., 97*, 3977, 1992.

Goertz, C. K., E. Nielsen, A. Korth, K. H. Glassmeier, C. Haldoupis, P. Hoeg, and D. Hayward, Observations of a possible ground signature of flux transfer events, *J. Geophys. Res., 90*, 4069, 1985.

Greenwald, R. A., et al., DARN/SuperDARN: A global view of the dynamics of high-latitude convection, *Space Sci. Rev., 71*, 761, 1995.

Hughes, W. J., and M. J. Engebretson, MACCS: Magnetometer array for cusp and cleft studies, in *Satellite - Ground Based Coordination Sourcebook*, edited by M. Lockwood et al., *Eur. Space Agency Spec. Publ., SP-1198*, 119, 1997.

Kivelson, M. G., and D. J. Southwood, Ionospheric traveling vortex generation by solar wind buffering of the magnetosphere, *J. Geophys. Res., 96*, 1661, 1991.

Konik, R. M., L. J. Lanzerotti, A. Wolfe, C. G. Maclennan, and D. Venkatesan, Cusp latitude magnetic impulse events, 2, Interplanetary magnetic field and solar wind conditions, *J. Geophys. Res., 99*, 14,831, 1994.

Konik, R. M., L. J. Lanzerotti, C. G. Maclennan, A. Wolfe, and D. Venkatesan, Cusp latitude magnetic impulse events, 3, Associated low-latitude signatures, *J. Geophys. Res., 100*, 7731, 1995.

Korotova, G. I., D. G. Sibeck, T. J. Rosenberg, C. T. Russell, and E. Friis-Christensen, High-latitude ionospheric transient events in a global context, *J. Geophys. Res., 102*, 17,499, 1997.

Lanzerotti, L. J., Conjugate spacecraft and ground-based studies of hydromagnetic phenomenon near the magnetopause, *Adv. Space Res., 8*(9-10), 301, 1988.

Lanzerotti, L. J., L. C. Lee, C. G. Maclennan, A. Wolfe, and L. V. Medford, Possible evidence of flux transfer events in the polar ionosphere, *Geophys. Res. Lett., 13*, 1089, 1986.

Lanzerotti, L. J., R. D. Hunsucker, D. Rice, L. C. Lee, A. Wolfe, C. G. Maclennan, and L. V. Medford, Ionosphere and ground-based response to field-aligned currents near the magnetospheric cusp regions, *J. Geophys. Res., 92*, 7739, 1987.

Lanzerotti, L. J., A. Wolfe, and N. Trivedi, Magnetic impulse events at high latitudes: Magnetopause and boundary layer plasma processes, *J. Geophys. Res., 95*, 97, 1990.

Lanzerotti, L. J., R. M. Konik, and A. Wolfe, Cusp latitude magnetopause events, 1, Occurrence statistics, *J. Geophys. Res., 96*, 14,009, 1991.

Lee, L. C., and Z. F. Fu, A theory of magnetic flux transfer at the earth's magnetopause, *Geophys. Res. Lett., 12*, 105, 1985.

Lin, Z. M., E. A. Bering, J. R. Benbrook, B. Liao, L. J. Lanzeroti, C. G. Maclennan, A. N. Wolfe, and E. Friis-Christensen, Statistical studies of impulsive events at high latitudes, *J. Geophys. Res., 100*, 7553, 1995.

Lockwood M., and J. Moen, Reconfiguration and closure of lobe flux by reconnection during northward IMF: Possible evidence for signatures in cusp/cleft auroral emissions, *Ann. Geophys., 17*, 996, 1999.

Lockwood, M., M. F. Smith, C. J. Farrugia, and G. L. Siscoe, Ionospheric ion upwelling in the wake of flux transfer events at the dayside magnetopause, *J. Geophys. Res., 93*, 5641, 1988.

Lühr, H., and W. Blawert, Ground signatures of traveling convection vortices, in *Solar Wind Sources of Magnetospheric Ultra-Low Frequency Waves, Geophys. Monogr. Ser.*, vol. 81, edited by M. J. Engebretson, K. Takahashi, and M. Scholer, p. 231, AGU, Washington, D. C., 1994.

Lühr, H., M. Lockwood, P. E. Sandholt, T. L. Hansen, and T. Moretto, Multi-instrument ground-based observations of a traveling convection vortices event, *Ann. Geophys., 14*, 162, 1996.

Lühr, H., M. Rother, T. Iemori, T. L. Hansen, and R. P. Lepping, Superposed epoch analysis applied to large-amplitude traveling vortices, *Ann. Geophys., 16*, 743, 1998.

McHenry, M. A., and R. C. Clauer, Modeled ground magnetic signatures of flux transfer events, *J. Geophys. Res., 92*, 11,231, 1987.

Mende, S. B., R. L. Rairden, L. J. Lanzerotti, and C. G. Maclennan, Magnetic impulse events and associated optical signatures in the dayside aurora, *Geophys. Res. Lett., 17*, 131, 1990.

Moretto, T., E. Friis-Christensen, H. Lühr, and E. Zesta, Global perspective of ionospheric traveling convection vortices: Case studies of two GEM events, *J. Geophys. Res., 102*, 11,597, 1997.

Newell, P. T., and C.-I., Meng, Mapping the dayside ionosphere to the magnetosphere according to particle precipitation characteristics, *Geophys. Res. Lett., 19*, 609, 1992.

Pinnock, M., A. S. Rodger, J. R. Dudeney, R. A. Greenwald, and K. B. Baker, An ionospheric signature of possible enhanced magnetic field merging on the dayside magnetopause, *J. Atmos. Terr. Phys., 53*, 201, 1991.

Potemra, T. A., L. J. Zanetti, K. Takahashi, R. E. Erlandson, H. Lühr, G. T. Marklund, L. P. Block, L. G. Blomberg, and R. P. Lepping, Multi-satellite and ground-based observations of transient ULF waves, *J. Geophys. Res., 94*, 2543, 1989.

Roelof, E. C., and D. G. Sibeck, Magnetopause shape as a bivariate function of interplanetary magnetic field B_z and solar wind dynamic pressure, *J. Geophys. Res., 98*, 21,421, 1993.

Rosenberg, T. J., and J. A. Doolittle, Studying the polar ionosphere and the magnetopause with automatic geophysical observatories: The U. S. program in Antarctica, *Antarct. J. U. S., 29*(5), 347, 1994.

Rosenberg, T. J., Z. Wang, A. S. Rodger, J. R. Dudeney, and K. B. Baker, Imaging riometer and HF radar measurements of drifting F region electron density structures in the polar cap, *J. Geophys. Res., 98*, 7757, 1993.

Sandholt, P. E., M. Lockwood, T. Oguti, S. W. H. Cowley, K. S. C. Freeman, B. Lybekk, A. Egeland, and D. M. Willis, Midday auroral breakup events and related energy and momentum transfer from the magnetosheath, *J. Geophys. Res., 95*, 1039, 1990.

Sato, M., H. Fukunishi, L. J. Lanzerotti, and C. G. Maclennan, Magnetic impulse events and related Pc1 bursts observed by the Automatic Geophysical observatories network in Antarctica, *J. Geophys. Res., 104*, 19,971, 1999.

Saunders, M. A., C. T. Russell, and N. Sckopke, Flux transfer events – Scale size and interior structure, *Geophys. Res. Lett., 11*, 131, 1984.

Schwartz, S. J., and D. Burgess, Quasi-parallel shocks: A patchwork of three-dimensional structures, *Geophys. Res. Lett., 18*, 373, 1991.

Sibeck, D. G., A model for the transient magnetospheric response to sudden solar wind dynamic pressure variations, *J. Geophys. Res., 95*, 3755, 1990.

Sibeck, D. G., Transient events in the outer magnetosphere: Boundary waves or flux transfer events?, *J. Geophys. Res., 97*, 4009, 1992.

Sibeck, D. G., Transient magnetic field signatures at high latitude, *J. Geophys. Res., 98*, 4009, 1993.

Sibeck, D. G., and D. J. Croley Jr., Solar wind dynamic pressure variations and possible ground signatures of flux transfer events, *J. Geophys. Res., 96*, 1669, 1991.

Sibeck, D. G., and G. I. Korotova, Occurrence patterns for transient magnetic field signatures at high latitudes, *J. Geophys. Res., 101*, 13,413, 1996.

Southwood, D. J., Theoretical aspects of ionosphere-magnetosphere-solar wind coupling, in physics of the ionosphere-magnetosphere, *Adv. Space Res., 5*(4), 4, 1985.

Southwood, D. J., The ionospheric signature of flux transfer events, *J. Geophys. Res., 92*, 3207, 1987.

Stauning, P., Absorption of cosmic noise in the E-region during electron heating events. A new class of riometer absorption events, *Geophys. Res. Lett., 11*, 1184, 1984.

Tamao, T., A hydromagnetic interpretation of geomagnetic SSC, *Rep. Ionos. Space Res. Jpn., 18*, 16-24, 1964.

Vorobjev, V. G., V. L. Zverev, and G. V. Starkov, Geomagnetic impulses in the daytime high latitude region: Main morphological characteristics and association with the dynamics of the daytime aurora, *Geomagn. Aeron.*, Engl. Transl., *33*, 621, 1994.

Vorobjev, V. G., O. I. Yagodkina, and V. L. Zverev, Morphological features of bipolar magnetic impulse events and associated interplanetary medium signatures, *J. Geophys. Res., 104*, 4595, 1999.

J. H. Doolittle, Space Physics Laboratory, O/L9-42 Lockheed Martin Advanced Technology Center, CA 94304-1191.

H. U. Frey, and S. B. Mende, Space Science Laboratory, University of California, Berkeley, CA 94720-7450.

H. Fukunishi, and R. Kataoka, Department of Geophysics, Tohoku University, Sendai, Miyagi, 980-8578, Japan. (ryuho@pat.geophys.tohoku.ac.jp)

L. J. Lanzerotti, and C. G. Maclennan, Bell Laboratories, Lucent Technologies, 600 Mountain Avenue, Murray Hill, NJ 07974-0636.

T. J. Rosenberg, and A. T. Weatherwax, Institute for Physical Science and Technology, University of Maryland, College Park, MD 20742-2431.

(Received August 9, 2000; revised April 19, 2001;
accepted April 23, 2001.)